EVALUATION OF LOCAL SITE AMPLIFICATION IN LIMA, PERU FROM GROUND MOTION DATA

Conference Paper · January 2017

CITATIONS
0

READS
243

7 authors, including:

Selene Quispe
National University of Engineering, Lima, Peru
10 PUBLICATIONS **11** CITATIONS
SEE PROFILE

Hiroaki Yamanaka
Tokyo Institute of Technology
191 PUBLICATIONS **1,040** CITATIONS
SEE PROFILE

Zenon Aguilar
Universidad Nacional de Ingeniería (Peru)
41 PUBLICATIONS **62** CITATIONS
SEE PROFILE

Fernando Lazares
Universidad Nacional de Ingeniería (Peru)
26 PUBLICATIONS **48** CITATIONS
SEE PROFILE

16th World Conference on Earthquake, 16WCEE 2017

Santiago Chile, January 9th to 13th 2017

Paper N° 3567

Registration Code: S-A1463232467

EVALUATION OF LOCAL SITE AMPLIFICATION IN LIMA, PERU FROM GROUND MOTION DATA

S. Quispe[(1)], H. Yamanaka[(2)], K. Chimoto[(2)], H. Tavera[(4)], Z. Aguilar[(5)], F. Lázares[(6)], and D. Calderón[(7)]

[(1)] *Researcher, Japan Peru Center for Earthquake Engineering and Disaster Mitigation, selene.quispe.g@uni.edu.pe*
[(2)] *Professor, Tokyo Institute of Technology, yamanaka@depe.titech.ac.jp*
[(3)] *Assistant professor, Tokyo Institute of Technology, chimoto.k.aa@m.titech.ac.jp*
[(4)] *Researcher, Geophysical Institute of Peru, hernando.tavera@igp.gob.pe*
[(5)] *Researcher, Japan Peru Center for Earthquake Engineering and Disaster Mitigation, zaguilar@zergeosystemperu.com*
[(6)] *Researcher, Japan Peru Center for Earthquake Engineering and Disaster Mitigation, f_lazares@uni.edu.pe*
[(7)] *Researcher, Japan Peru Center for Earthquake Engineering and Disaster Mitigation, dcalderon@uni.edu.pe*

Abstract

Observed ground motion records were analyzed for estimating site effects in Lima Metropolitan Area, Peru in the frequency range from 1.0 to 20.0 Hz. The spectral inversion method was applied to separate the three effects – path, source and site amplification. This technique is the most appropriate for analyzing site response since amplification is only attributed to the effect of sedimentary soil layers over a basement. The earthquake data used were 55 seismic events observed at 19 seismic recording stations from 2003 to 2013. Most of the earthquakes used in the analysis were small events with a Local Magnitude ML between 4.0 and 5.0. The estimated S-wave quality factor (Qs) of the propagation path is modelled as $Qs(f)=95.6f^{0.66}$ for the crust and mantle. This study characterizes the site response for the predominant subsurface soil formations over Lima such gravels, sands and clays. Stations installed on alluvial gravel deposits or locally known as Lima conglomerate tend to amplify at frequencies higher than 3 Hz. This material has S-wave velocities increasing gradually with depth from ~400 to ~1500 m/s. The site response of stations installed on sand and clay deposits control the amplification in a wide frequency range. Large amplification factors in the frequency range over 5 Hz is attributed to the effects of the top layers – sands and clays – with Vs ranging between ~100 to ~500 m/s, while amplification factors at frequencies lower than 5 Hz correspond to the high velocity contrast between the shallow and deep layers (Vs > ~800 m/s).

Keywords: Lima; Callao; site effects; spectral inversion method.

1. Introduction

Lima Metropolitan Area or Lima is the name given to the area formed by the Province of Lima and the Province of Callao. This place has the highest population over Peru mainly due to the fact that Lima Province is the capital of Peru. A quick growing of population is expected to occur in the following years [1]. Lima is situated in one of the seismically active regions, due to the subduction of the Nazca Plane beneath the South American Plate. Historical records show that large and great earthquakes (Mw>7.5) have struck along Lima Metropolitan Area. One of the most destructive events occurred in 1746 with a moment magnitude of ~8.8 [2]. Based on the studies of Dorbath et al. (1990) [2], Sladen et al. (2010) [3], and Pulido et al. (2012) [4], a 1746 event like-megathrust earthquake is likely to affect Lima Metropolitan Area in the near future. The estimated moment magnitude for this very large event might be larger than 8.8. Therefore, earthquake disaster mitigation is one of the important issues in Lima Metropolitan Area due to the impact that this natural disaster might have on Peruvian society regarding human losses and building damage.

Seismic zoning maps have already been proposed for Lima [5, 6]. In the zonation maps, areas which are prone to amplify seismic waves due to the local soil conditions have been mapped, however these maps have certain limitations that result from the nature of regional mapping, data limitations, and generalization. The assessment of observed site amplification using ground motion records is still in its preliminary stages mainly due to the lack of knowledge, the limitation in data, and the access to it [7 – 9]. Quispe et al. (2013) [9] applied the Spectral Inversion Method (SIM) [10] to earthquake recordings observed along the Pacific coast of Lima, Peru, for site response estimation. The information used was limited regarding the number of earthquake stations and consequently the number of seismic records, so their study stresses to reanalyze their results with new data in order to have a better understanding how the subsurface condition controls the factors of site amplification in the frequency range of interest [9].

The present work adds data of other stations and events to those analyzed by Quispe et al. (2013) [9]. Then, the spectral inversion method is applied to the new data-set to evaluate the local site effects. The benefit of SIM is that it can separate site, path and source effects from S-wave spectra. The influence of subsurface soil on site response is discussed in the present paper. The site effect evaluation includes stations located at La Molina, Villa El Salvador and Callao, places where seismic waves are prone to amplify due to the local soil conditions [2 – 9, 11, 13, 14].

2. Geological and Geomorphological Aspects

The geology of Lima Metropolitan Area reflects the complex tectonic process that Lima has been subjected in the past due to the subduction of Nazca Plate beneath South American Plate. Fig. 1a shows geological map of Lima Metropolitan Area [15]. Part of Andes Cordillera is observed in the eastern part of Lima. The geologic units of Andes Cordillera within Lima are mainly composed of sedimentary and intrusive rocks from the Cretaceous age. Cretaceous deposits from Puente Piedra Group appear to the northwest of Lima, while deposits from Morro Solar Group are exposed in the southwest of the city. Rocks from Casma Group outcrop in many parts of the city, and intrusive rocks are found exposed mainly in the eastern part of the study area.

The Lima coastal plain is found between the Andes Cordillera and the Pacific Ocean. According to the literature [5, 11, 12], the plain lies on Alluvial fan deposits of Chillón and Rímac Rivers as displayed in Fig. 1a. Both rivers have eroded deep valleys on the coastal plain in the past; especially Rímac River has had a big contribution in the formation of the plain, due to its short length, steep gradient and considerable flow. In the geologic past, a considerable amount of large-diameter material was transported from Andes Cordillera – the origin of the rivers – to the sea level. This material corresponds to the Quaternary deposits of Lima as shown in Fig. 1a. Most of the Lima's population is concentrated in this area.

The geological map of Lima shows the Quaternary deposits are composed of alluvial, marine, and aeolian material. The distribution of the alluvial material is very wide. The alluvial deposits extend from the ground's surface to the rock, and mainly consist of medium dense to very dense coarse gravel and sand with cobbles,

locally known as Lima Conglomerate. The thickness of this material (to the basement) is reported to be over 100 m, with S-wave velocities ranging from ~500 to ~1500 m/s gradually increasing with depth [7, 11, 13].

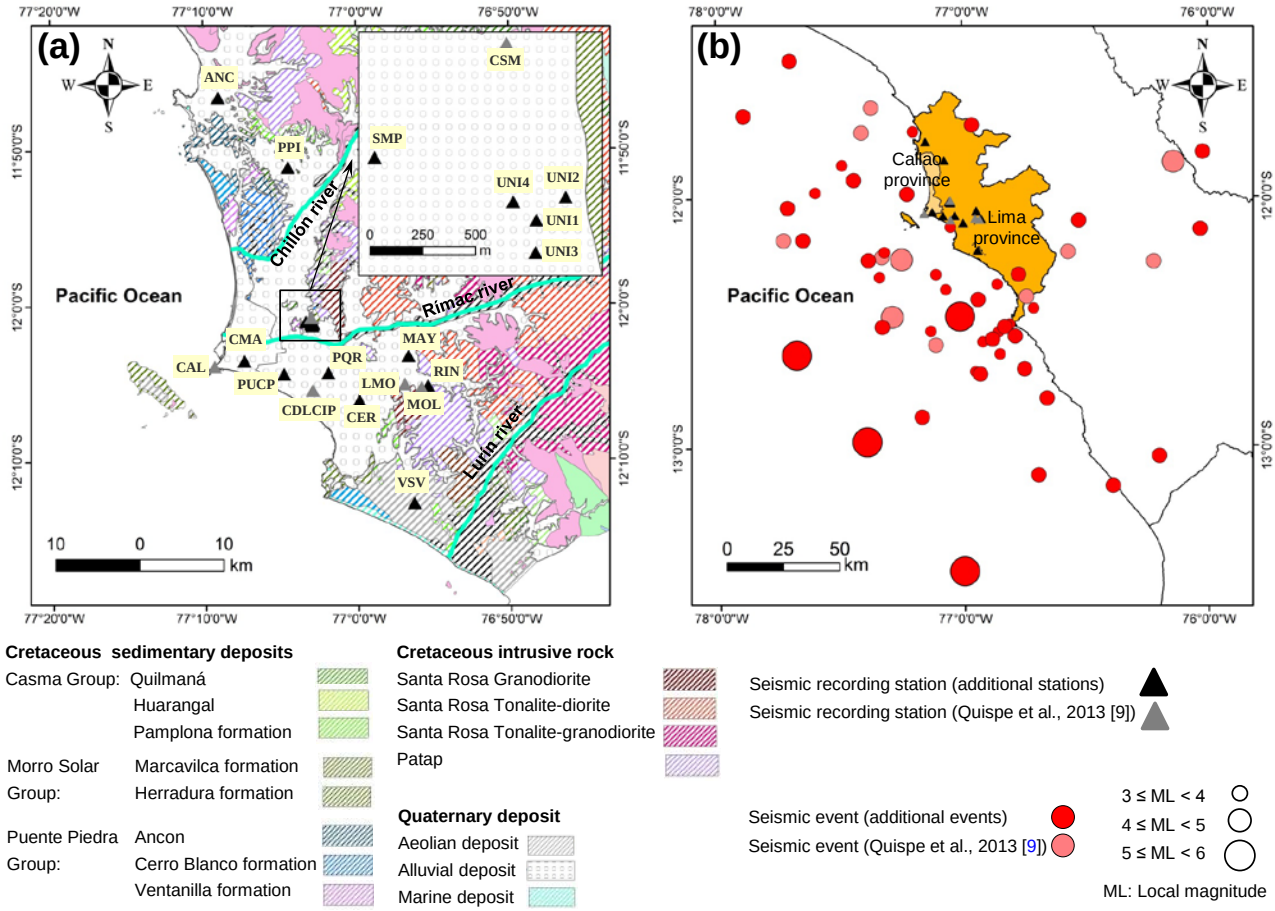

Fig. 1 – Study area with location of stations and epicenters. (a) Geological map of Lima [15] with location of earthquake stations. Black triangles represent new stations included in this study, while grey triangles represent stations previously analyzed by Quispe et al. (2013) [9]. (b) Lima Metropolitan Area with epicenter of seismic events. Dark red circles mean the epicenter of new events, while light red colors represent the earthquakes analyzed in this previous study [9].

3. Earthquake Observation and Ground Motion Records

The strong motion network at Lima Metropolitan Area has been expanded continuously during the past decade [14]; being currently operated by two institutions: the Geophysical Institute of Peru (IGP) and the Japan-Peru Center for Earthquake Engineering, Research, and Disaster Mitigation (CISMID). Fig. 1a shows the location of the nineteen recording sites used in the study. Stations indicated by black triangles are additional ones used in the present study, while those indicated by grey triangles are the same as those used previously by Quispe et al. (2013) [9]. Site response of 14 new sites is been analyzed in this work, a part of the 5 stations previously analyzed by Quispe et al. (2013) [9]. Fig. 1a shows all the stations are located on Quaternary deposits, less the LMO site located on intrusive rock. This rock station served as a reference site to estimate site amplification effects in the present study. Table 1 gives pertinent information on the earthquake stations related to each station's name, location, observation institution, geographical coordinates, and geology.

Table 1 – List of earthquake stations.

Station ID	Location		Institution	Latitude	Longitude	Geology
	District	Province		(deg)	(deg)	
CSM	Rímac	Lima	CISMID	-12.013	-77.050	Quaternary Alluvial
CAL	Callao	Callao	CISMID	-12.066	-77.156	Quaternary Alluvial
MOL	La Molina	Lima	CISMID	-12.089	-76.930	Quaternary Alluvial
CDLCIP	San Isidro	Lima	CISMID	-12.092	-77.049	Quaternary Alluvial
LMO	La Molina	Lima	IGP	-12.085	-76.948	Santa Rosa Granodiorite
ANC	Ancón	Lima	IGP	-11.777	-77.150	Quaternary Alluvial
PUCP	San Miguel	Lima	IGP	-12.074	-77.080	Quaternary Alluvial
RIN	La Molina	Lima	IGP	-12.087	-76.923	Quaternary Alluvial
CER	San Borja	Lima	IGP	-12.103	-76.998	Quaternary Alluvial
MAY	Ate	Lima	IGP	-12.055	76.944	Quaternary Alluvial
UNI1	Rímac	Lima	CISMID	-12.021	-77.049	Quaternary Alluvial
UNI2	Rímac	Lima	CISMID	-12.020	-77.048	Quaternary Alluvial
UNI3	Rímac	Lima	CISMID	-12.022	-77.049	Quaternary Alluvial
UNI4	Rímac	Lima	CISMID	-12.020	-77.050	Quaternary Alluvial
VSV	Villa El Salvador	Lima	CISMID	-12.213	-76.938	Quaternary Marine
PQR	Lima	Lima	CISMID	-12.073	-77.032	Quaternary Alluvial
SMP	San Martín de Porres	Lima	CISMID	-12.018	-77.056	Quaternary Alluvial
PPI	Puente Piedra	Lima	CISMID	-11.852	-77.074	Quaternary Alluvial
CMA	Bellavista	Callao	CISMID	-12.060	-77.123	Quaternary Alluvial

The strong motion network has recorded hundreds of events in the last ten years. In this study, we analyzed 55 moderate earthquakes observed at the 19 seismic recording stations from 2003 to 2013, including the same events as those analyzed by Quispe et al. (2013) [9]. Fig 1b shows the epicenters of the analyzed events. Dark red circles indicate new events, while light red circles indicate events previously used by Quispe et al. (2013) [9]. A total of 232 ground motion records were processed in this study. Fig. 2 shows the hypocentral distribution of them with depth represented by black points. The grey points indicate the records used in this previous study [9], also analyzed in the present work. 201 seismic records more have been included in the analysis. The data set used (black points) shows a better coverage over hypocentral distance than those analyzed by Quispe et al. (2013) [9] (grey points), as displayed in Fig. 2. The additional new events as well as the previous events analyzed by Quispe et al. (2013) [9] are shallow and intermediate earthquakes (depth < 140 km). The hypocentral distance of them is in the range between 40 Km and 200 Km. Table 2 presents the earthquake parameters determined by the Geophysical Institute of Peru (IGP).

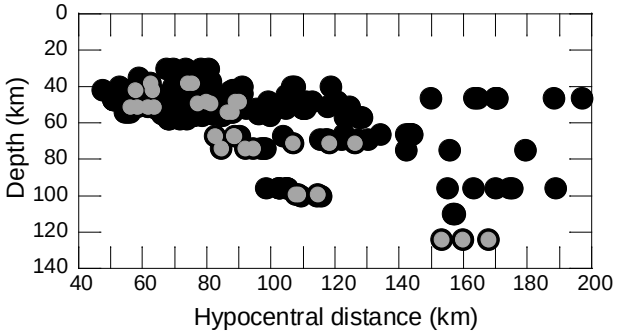

Fig. 2. Distribution of hypocentral distance and depth. The present work has analyzed 232 seismic records represented by black points. Grey points represent the records previously analyzed by Quispe et al. (2013) [9], also included in this study.

Table 2. Seismic event information.

Date	Hour	Long.	Lat.	Mag.	Depth	Earthquake stations																		
yyyy/mm/dd	hr:min	(deg)	(deg)	(ML)	(km)	CSM	CAL	MOL	CDLCIP	LMO	ANC	PUCP	RIN	CER	MAY	UNI1	UNI2	UNI3	UNI4	VSV	PQR	SMP	PPI	CMA
08/05/2003	16:33	-77.395	-12.980	5.4	51	*						*												
28/05/2003	21:26	-77.013	-12.479	5.3	51	*						*												
02/03/2005	13:48	-76.140	-11.860	5.7	124	*	*	*																
2005/07/19	13:45	-77.110	-12.590	4.1	49	*		*																
25/07/2005	06:51	-77.330	-12.240	4.0	42	*		*			*													
14/10/2005	05:01	-76.740	-12.400	4.4	74	*	*	*																
2005/11/10	16:38	-76.220	-12.260	4.0	71	*	*	*																
2005/12/27	17:02	-76.570	-12.220	4.5	99	*		*																
2006/05/26	01:57	-77.410	-11.740	4.5	38	*		*		*														
11/12/2006	21:53	-77.370	-11.640	4.2	54			*		*			*											
2008/03/29	06:40	-77.730	-12.170	4.3	48	*	*		*						*									
2008/03/29	12:51	-77.250	-12.250	5.3	51	*	*		*	*	*		*		*									
2008/06/07	13:06	-77.290	-12.480	5.0	67	*	*			*	*				*									
02/10/2011	16:33	-76.880	-12.570	4.0	74	*											*							*
20/11/2011	03:00	-77.490	-11.870	3.9	56											*	*		*					
19/12/2011	05:37	-77.385	-12.252	4.7	44	*							*			*	*	*	*		*		*	
26/12/2011	20:29	-76.659	-12.807	4.4	52	*											*	*	*	*	*			
29/12/2011	13:45	-76.788	-12.558	4.6	52	*										*	*	*		*	*		*	*
23/01/2012	02:31	-77.713	-12.040	4.4	37	*																*		
11/02/2012	04:27	-76.695	-13.116	4.8	66	*							*			*	*	*		*		*		*
14/02/2012	04:42	-76.938	-12.411	4.8	42	*										*	*	*	*	*	*	*	*	*
19/02/2012	02:19	-77.225	-11.987	4.0	47	*							*				*	*	*		*	*		
29/02/2012	08:50	-76.750	-12.690	4.3	40	*							*							*				
07/03/2012	03:52	-77.110	-12.310	3.7	49						*									*	*	*	*	
11/03/2012	08:20	-77.132	-12.537	3.8	52															*	*		*	
19/03/2012	23:21	-77.442	-11.931	4.0	45						*		*			*	*	*	*					
25/03/2012	23:00	-77.680	-12.630	5.0	48					*	*		*			*	*	*				*		
17/05/2012	03:45	-76.526	-12.095	4.2	100	*							*					*			*			
21/06/2012	22:17	-76.960	-11.710	4.7	96	*				*	*		*					*			*	*		*
27/06/2012	12:41	-76.200	-13.040	4.2	96								*					*		*	*	*	*	
28/06/2012	11:18	-77.650	-12.170	4.2	44					*	*		*		*			*			*	*		*
04/07/2012	16:01	-77.050	-12.120	3.8	54						*		*								*	*		
16/07/2012	17:21	-76.860	-12.350	3.8	40										*	*		*				*		
01/08/2012	13:02	-77.340	-12.320	3.7	46					*	*		*		*			*			*	*	*	
07/08/2012	10:30	-77.000	-13.500	5.4	46						*		*				*	*		*	*	*	*	
11/08/2012	09:35	-77.700	-11.450	4.3	69								*		*		*	*			*	*		*
15/09/2012	11:27	-77.330	-12.520	4.0	47								*	*	*		*	*		*	*	*		
25/09/2012	06:50	-77.320	-12.220	3.9	42								*	*	*		*	*			*	*		
14/10/2012	16:50	-77.600	-11.980	3.7	30					*			*	*			*	*			*			
30/10/2012	07:48	-76.855	-12.540	3.9	52								*	*			*	*		*	*	*	*	
30/10/2012	13:35	-76.920	-12.580	3.9	56								*				*			*			*	
30/10/2012	19:44	-76.830	-12.520	4.3	55					*			*	*	*		*	*		*	*	*	*	
01/11/2012	01:37	-76.020	-11.820	4.5	57												*	*		*	*	*		
04/11/2012	01:52	-76.030	-12.130	4.7	110												*	*				*		
05/11/2012	08:08	-76.810	-12.510	3.9	50												*	*			*			
10/11/2012	06:57	-76.712	-12.446	3.9	45												*			*		*	*	
10/01/2013	05:14	-77.890	-11.670	4.2	40											*		*	*					
15/01/2013	19:01	-77.070	-12.370	3.9	48											*		*	*	*	*	*		
01/03/2013	02:56	-76.950	-12.700	3.9	43											*				*				
02/03/2013	02:51	-76.930	-12.710	4.1	42											*				*		*		
05/03/2013	04:24	-76.850	-12.630	3.8	35											*		*		*				
11/03/2013	14:33	-77.170	-12.881	4.2	45										*	*				*				
19/03/2013	23:06	-76.390	-13.160	4.6	75										*					*			*	
12/04/2013	13:53	-77.201	-11.736	3.8	58										*			*			*	*		
10/05/2013	03:35	-76.772	-12.311	4.3	52													*		*	*			

The data surrounded with dense lines are those analyzed by Quispe et al. (2013) [9]

Source parameters were determined by the Geophysical Institute of Peru (IGP)

(* means that the event was recorded)

The procedure for calculating S-wave spectra was the same as followed by Quispe et al. (2013) [9]. First, S-wave portion of two horizontal components, EW and NS, was selected, beginning at initial shear-wave arrival. For recognizing the onset time of S-wave, Husid plots [16] were used, where horizontal axis is the time and vertical axis is the accumulated horizontal component square for each horizontal component. The end moment of S-wave was picked up by using cumulative Root Mean Square (RMS) function [17]. In this study, the time at which the S-wave window ended was defined as the point on the time axis at which cumulative RMS starts to decrease. The end moment of S-wave was estimated visually.

After the onset and end times of S-wave were determined, the S-wave portion was cosine-tapered 10 percent at each end of the time window, using the same criterion as that used by Takemura et al. (1990) [18]. The horizontal spectrum was then calculated, using the Fast Fourier Transform. Spectral amplitudes were smoothed with a 1.2 Hz-width Parzen window. Next, S-wave Fourier amplitude spectra of two horizontal components were summed vectorially for being used in the analysis.

Most of the analyzed seismic events were small with a length of S-waves from 2 to 4 s, offering a low resolution for frequencies lower than 1 Hz. Therefore, site, path, and source effects were evaluated in the frequency range from 1.0 to 20.0 Hz in the present work.

4. Spectral Inversion Method

4.1 Methodology

The earthquake records were analyzed by the Spectral Inversion Method (SIM) [10], in order to estimate effects of site response, path and source spectra. From a practical point of view, this technique offers the advantage that records from some events can be included in the inversion even if these events are not recorded at all sites. This offers the advantage of a more complete exploitation of the data set [19].

The observed S-wave Fourier amplitude spectra of the i^{th} event recorded at the j^{th} site $O_{ij}(f)$ can be written in the frequency domain as a linear multiplication of a site-effect term $G_j(f)$, a path term $P_{ij}(f,R)$, and a source term $S_i(f)$:

$$O_{ij}(f) = G_j(f).P_{ij}(f,R).S_i(f) \quad (1)$$

The path effect includes two factors in the case of point source assumption: one is the geometrical spreading, which can be expressed by means of R_{ij}^{-1}, and the other is the inelastic losses. The path effect term $P_{ij}(f,R)$ can be represented as follows:

$$P_{ij}(f) = R_{ij}^{-1}.\exp(-\pi R_{ij} f/Qs(f)Vs) \quad (2)$$

where R_{ij} is the hypocentral distance between the i^{th} event and the j^{th} station, Qs(f) and Vs are S-wave frequency dependent quality factor and velocity along the wave propagation path, respectively. Note that Vs equal to 3.5 km/sec were assumed in this study. As a result, $O_{ij}(f)$ would be represented as:

$$O_{ij}(f) = G_j(f).R_{ij}^{-1}.\exp(-\pi R_{ij} f/Qs(f)Vs).S_i(f) \quad (3)$$

Performing a logarithmic operation to Eq. (3), simultaneous logarithm equations with unknown parameters of I (source spectrum) + J (site effect) + 1 (Qs-value) from I×J data for each frequency are obtained. The unknown parameters can be solved by using the singular value decomposition method [20], however there is still one undetermined degree of freedom. To solve the undetermined degree of freedom in the equations, a constraint condition should be given by choosing at least one reference site or event. This study used a reference site. Many authors [21 – 23] used a rock site as a constraint condition by constraining its site response. The site response was computed numerically by one-dimensional vertical multiple reflection of S waves, as well as geological and geotechnical information was consulted since rock sites suffer from local site effects.

4.2 Constraint condition

As discussed above, a constraint condition is needed to remove the undetermined degree of freedom in the inversion process. The site response of an outcropping rock site coded LMO was chosen as constraint condition; LMO site is the only station located on rock. A geophysical exploration using Multichannel Analysis of Surface Waves (MASW) method was performed at this site to define the Vs structure; no dynamic information was previously available for this station. The estimated Vs profile reached a depth of 30 m, where the bottom layer had a S-wave velocity of ~2200 m/s, as shown in Fig. 3a. Fig. 3b displays the site response of LMO calculated numerically, estimated from the profile. Slight amplification is observed at frequencies higher than 9 Hz. The theoretical site amplification of LMO was the constraint condition in the present work, free surface effects were considered. Additionally, microtremor measurements were also conducted to calculate the horizontal to vertical (H/V) spectral ratio [24]. Fig. 3c shows no strong peaks in the frequency of interest.

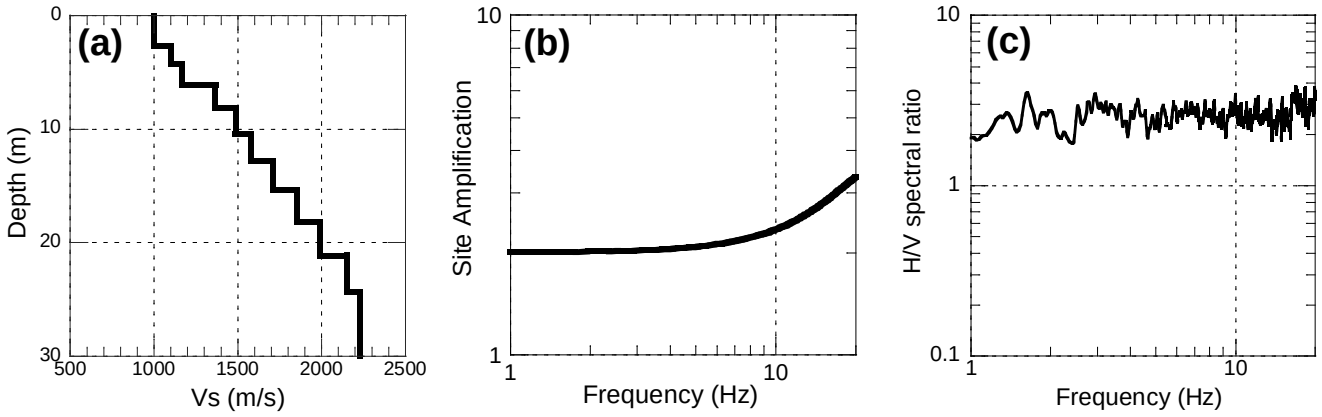

Fig. 3. Seismic information at LMO station. (a) S-wave velocity profile. (b) 1-D amplification of SH waves. (c) H/V spectral ratio of microtremor.

4.3 Qs-values for propagation path and source effects

S-wave quality factor, source spectra and site response were simultaneously obtained applying the inversion technique to the selected database. The estimated S-wave quality factor (Qs-values) denoted by points is shown in Fig. 4a. The black solid line in the figure is a regression line for $Qs(f)=95.6f^{0.66}$, while the grey line represents the quality factor estimated by Quispe et al. (2003) [9]. This study included new additional data, overcoming the limitation of data reported by Quispe et al. (2013) [9]. The data set used shows better coverage over hypocentral distance than those used by Quispe et al. (2013) [9] (Fig. 2), indicating Qs-values are more stable than those obtained by Quispe et al. (2003) [9]. The seismic records used in their study [9] only covered a limited hypocentral distance interval, as illustrated in Fig. 2. Fig. 4a also shows the estimated Qs factor is slightly larger than the previous results [9]. One possibility might be related to the analysis of new stations with much better spatial distribution (Fig. 1a), as well as the inclusion of more seismic events (Fig. 1b), as previously mentioned.

Source acceleration amplitude spectra $S_i(f)$ of the 55 events were obtained from the inversion analysis, and the seismic moment density function $M_i(f)$ for each event was calculated applying the equation also used in these studies [18, 25, 26]. The authors used the same coefficients as previously used in the study of Quispe et al. (2013) [9] for the calculation of $M_i(f)$. Fig. 4b displays three examples of computed $M_i(f)$ with different magnitudes. The amplification level of seismic moment depends significantly on magnitude as shown in Fig. 4a. The Brune's omega-square model [26] represented by solid lines in Fig. 4a was also calculated. The theoretical model can fit well the observed values in the frequency range between 1.0 and 10.0 Hz.

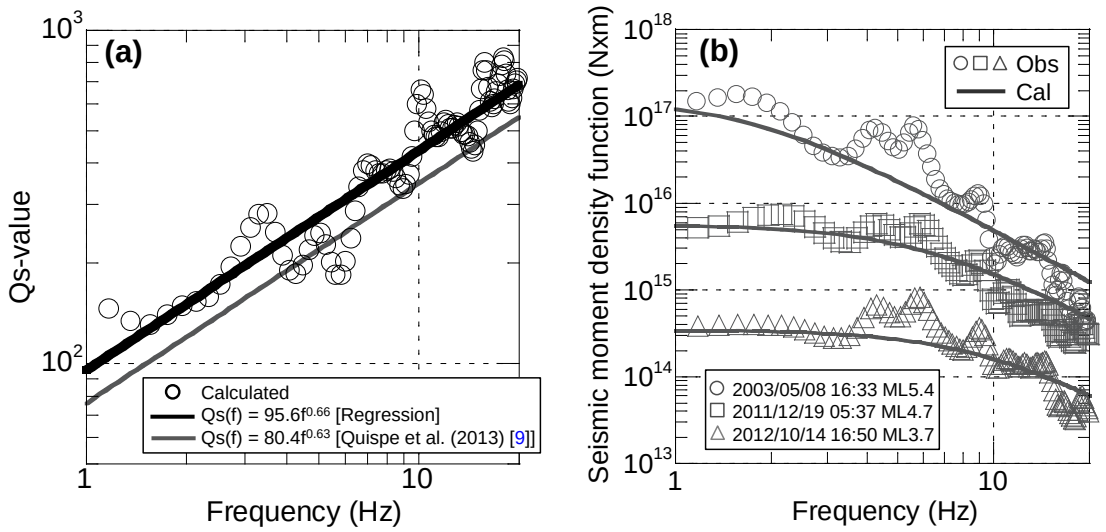

Fig. 4. (a) Qs-values determined by the inversion as a function of frequency. The black solid line represents the best-fit relation between Qs-values and frequency for the present study. The grey solid line indicates the result estimated by Quispe et al. (2013) [9]. (b) Examples of seismic moment density functions (open circles, squares and triangles) and approximated omega-squared model shown by solid lines.

4.4 Inverted site amplification

Fig. 5 displays the results related to site amplification obtained from the inversion technique in this study, represented by a black solid line. The results previously obtained by Quispe et al. (2013) [9] for CSM, CAL, MOL and CDLCIP sediment sites are also shown in Fig. 9, represented by a grey dash line. Differences are observed between each other. Quispe et al. (2013) [9] reported that their results still have difficulties in the solution because of the limitation in data, as previously explained. This study has overcome such limitation, indicating the site response estimated in this study is more stable in the frequency range of interest from 1 to 20 Hz.

The amplification estimated in this study is predominantly caused by the input motion of SH-waves propagating vertically from the bottom layer (Vs ~2200 m/s) of the model for the reference site. The inversion results (black solid lines) were also compared with the theoretical amplification from the 1-D S-wave profiles (grey solid lines). Shallow and deep Vs structure is known for CSM, CAL, ANC, PUCP, MAY, VSV, and CMA stations. They were estimated from microtremor measurements [7, 13]. The layer Vs ~ 2200 m/s was detected in all these models. The theoretical amplification for these sites was computed from this layer to the ground surface. Fig. 5 shows peaks and troughs of the theoretical site amplification can be identified in those of the spectral inversion technique, however amplification levels differ for some sites. The location where the microtremor observation was conducted is more than 50 m away from the site where the earthquake station is installed. This might explain the misfit between observed and calculated amplification factors.

From the inversion results obtained in this study, we observed that stations such as CSM, MOL, PQR, SMP, UNI1, UNI2, UNI3, and UNI4 mainly display the predominant peaks at frequencies higher than 3 Hz, while some sites such as ANC, RIN, VSV, and PPI show several predominant peaks with large amplification in a wide frequency range. On the contrary, the site response for CMA and CAL stations displays spectral decrease from low to high frequency. The reason why the factors of site amplification change in the frequency range is in relation to the subsurface condition. This is going to be explained in details in the following section.

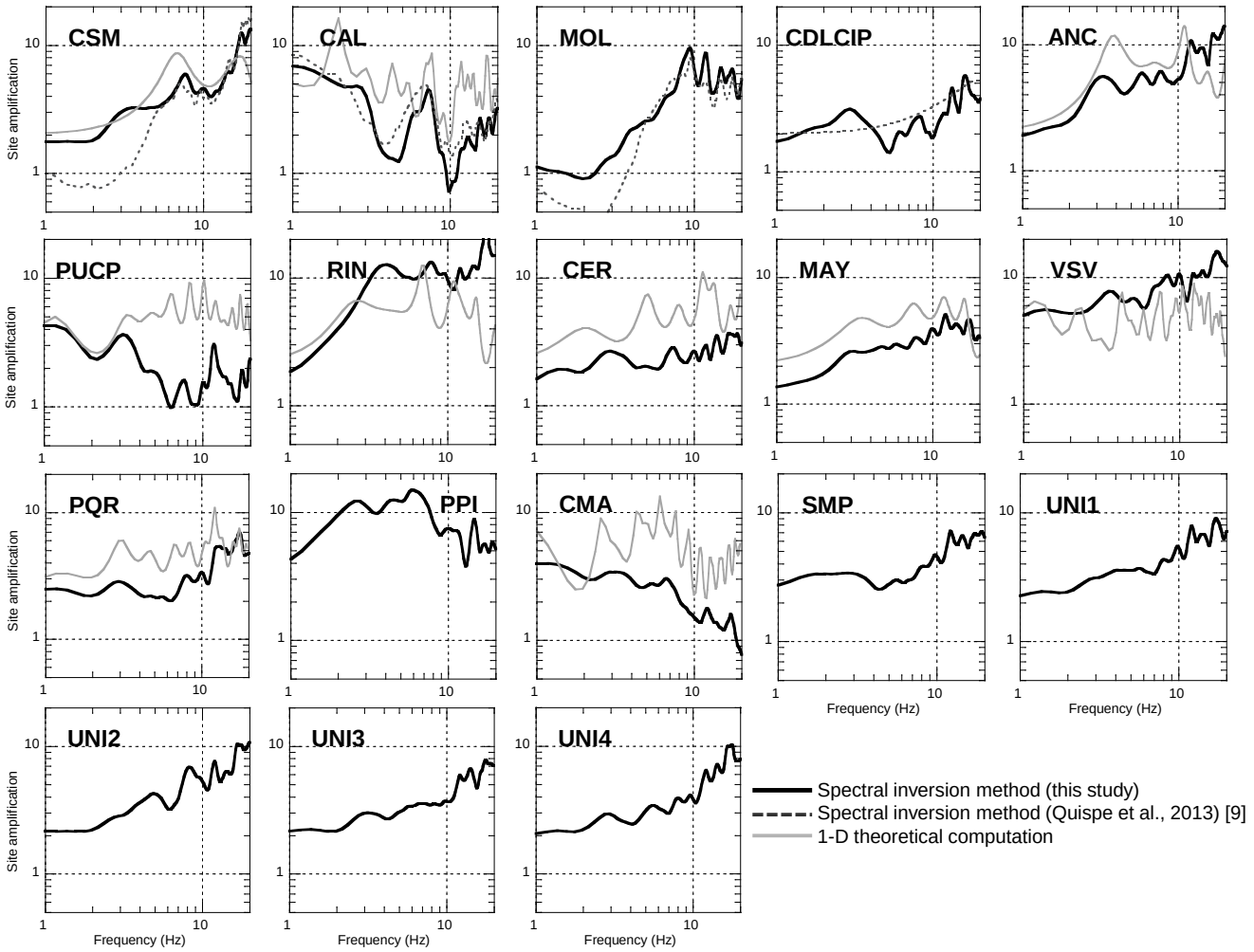

Fig. 5. Amplification factors at sediment sites calculated by the inversion technique and 1-D theoretical computation. The black solid lines represent the site response estimated in this study, while the grey dashed lines represent the results previously estimated by Quispe et al. (2013) [9]. The grey solid lines indicate the theoretical transfer function from the bottom layer (Vs ~2200 m/s) to the ground surface. Vs structure at MOL, SMP, UNI1, UNI2, UNI3, and UNI4 stations is unknown.

5. Discussion

5.1 Surface geology and local site amplification

The geological map of Lima shows all sediment sites are located on Quaternary deposits (Fig 1a), but the surface condition for each site differs. The predominant alluvial material over Lima Metropolitan Area is the Lima conglomerate. The distribution and properties of the various subsurface soils overlying the conglomerate are displayed in the soil distribution map of Lima proposed by CISMID (2005) [5]. The subsurface conditions were grouped into four soil types – gravels, silty sands, aeolian sands, and clays – to simplify the variety of soil materials [27].

According to this map [5], CSM, MOL, CDLCIP, PUCP, CER, PQR, SMP, UNI1, UNI2, UNI3 and UNI4 stations are located on alluvial gravel. All of them are installed in different districts of Lima province as presented in Table 1. These sites show the highest amplifications levels at frequencies above 3 Hz,

corresponding to the site response of the Lima conglomerate, previously reported by Quispe et al. (2013, 2014) [9, 13], as shown in Fig. 5. The Lima conglomerate extends from near the ground's surface to the bedrock, with S-wave velocities increasing gradually with depth from ~400 to ~1500 m/s [7, 11, 13].

RIN (La Molina district) and PPI (Puente Piedra district) sites are installed on layers of sand and silt overlying the Lima conglomerate [5]. These sites show several peaks at frequencies higher than 5 Hz (Fig. 5), representing the resonance between the top layers (Vs ranging within ~100 and ~500 m/s) and the alluvial deposits [13]. RIN and PPI sites also show dominant peaks with high amplification at frequencies below 5 Hz, attributed to the velocity contrast between the deep soil layers – underlying the engineering bedrock (Vs ~500 m/s) – and the top layers. This study as well as microtremor observations conducted at RIN and PPI sites [7, 13] reveal these stations are located on layers of sand and silt with a thickness larger than 10 m, in contrary to what CISMID (2005) [5] reported, so the soil classification map needs to be updated.

According to the soil distribution map, MAY station is also installed on silty sand deposits, but amplification factors at this site is similar to those in gravel deposits. Microtremor observations conducted at this site [13] as well as the results estimated in this study suggest this station might be located on alluvial gravels.

VSV station is situated on thick aeolian sand deposits [5, 7]. The soil formation is the predominant soil type in the Villa El Salvador district, where the VSV recording site is installed. Large amplification factors in the frequency range over 5 Hz is attributed to the effects of the deposit with Vs ranging from ~200 and ~500 m/s, while amplification factors at frequencies lower than 5 Hz correspond to the contribution of high velocity layers (Vs ~1000 m/s) underlying the engineering basement.

Fig. 5 shows the first resonance mode at ANC site is at a frequency between 3 and 4 Hz, also reported by Quispe et al. (2014) [13]. The soil distribution map of Lima proposed by CISMID (2005) [5] provides scarce information at this site, located on the outskirts of Lima – Ancón district. Available geotechnical reports show the surface condition at the ANC site is predominantly aeolian sand layers with S-wave velocities between ~200 and ~500 m/s [13].

Amplification levels at CMA site increase from high to low frequencies as shown in Fig. 5, and higher amplification is expected for frequencies lower than 1 Hz, also reported by Calderon et al. (2012) [7]. This study cannot define the amplification level for frequencies lower than 1 Hz because most of the analyzed S-wave Fourier Spectra are not so powerful at this frequency, as previously mentioned. The shallow soil condition at CMA shows two unconsolidated materials, a soft clay layer (Vs ~250 m/s) with a thickness of about 10 m, and a thick fine soil layer (Vs ~450 m/s). Stiff layers are found underlying these unconsolidated materials at a depth of ~150 m, with a Vs ranging from ~1000 to ~2500 m/s gradually increasing with depth [5, 7].

CAL site exhibits a dominant peak at a frequency of ~7 Hz, and also the amplification factor increases at frequencies below 5 Hz [7, 9], as shown in Fig. 5. The local site response at CAL represents the resonance between the ~25 m shallow materials (Vs ~250 m/s) and the high velocity layers (Vs larger than ~500 m/s). The shallow materials are mainly composed of clays, silts and sands [5, 11]. CAL and CMA stations are installed in Callao province. Historically large ground motions have been reported during important earthquakes in Callao because of the soil subsurface conditions [28].

6. Conclusions

Site response in Lima Metropolitan Area was evaluated at 19 seismic recording stations using actual observed ground motion data. The spectral inversion method was applied in order to separate path, source and site effects. The estimated Qs-value of the propagation path is modeled as $95.6f^{0.66}$. Source spectra can be approximated with the omega-squared model. Observed site response estimated in the present work are due to the effects of shallow and deep soils over a basement with an S-wave velocity of ~2200 m/s. Stations located on alluvial gravel deposits shows the Lima conglomerate amplifies to frequencies higher than 3.0 Hz, confirming what was previously reported by Quispe et al. (2013, 1014) [9, 13]. This material has S-wave velocities increasing gradually with depth from ~400 to ~1500 m/s. The sand deposits (silty and aeolian sands) amplify in a wide frequency range. Large amplification factors in the frequency range over 5 Hz is attributed to the effects of the

top layers – sands – with Vs ranging from ~100 to ~500 m/s, while amplification factors at frequencies lower than 5 Hz correspond to the high velocity contrast the top and high velocity layers (Vs > ~800 m/s). The clay deposits also control the amplification in a wide frequency range, but clays have the particular characteristic of amplifying from high to low frequency compared to sands. The shallow layers are mainly composed of clays with Vs varying between ~100 and ~500 m/s, this material controls the amplification at frequency higher than 5 Hz. Large amplification at frequencies lower than 5 Hz is the result of the high velocity contrast between the shallow and deep layers (Vs > ~1000 m/s). This study strongly recommends analyzing seismic events with large S-wave portion in order to define the amplification at this frequency range. This study contributes to the understanding of local site effects in areas such as Villa El Salvador and Ancón districts, places where the dynamic information is still scarce, so the soil distribution and microzonation maps [5, 6] should be updated using as a reference this work.

7. Acknowledgements

We would like to express our sincere gratitude to Dr. Hussam Eldein Zaineh from Tokyo Institute of Technology for the comments and discussions who helped to improve this manuscript.

8. References

[1] Dirección Técnica de Demografía e Indicadores Sociales (2012): Perú: Estimaciones y Proyecciones de Población Total por Sexo de las Principales Ciudades, 2000 – 2015. *Instituto Nacional de Estadística e Informática (INEI)* (In Spanish).

[2] Dorbath L, Cisternas A, and Dorbath C (1990): Assessment of the Size of Large and Great Historical Earthquakes in Peru. *Bulletin of the Seismological Society of America*, Vol. 80, No. 3, pp. 551-576.

[3] Sladen A, Tavera H, Simons M, Avouac JP, Konca AO, Perfettini H, Audin L, Fielding EJ, Ortega F, and Cavagnoud R (2010): Source Model of the 2007 Mw 8.0 Pisco, Peru Earthquake: Implications for Seismogenic Behavior of Subduction Megathrusts. *Journal of Geophysical Research*, Vol. 115, B02405, doi:10.1029/2009JB006429.

[4] Pulido N, Tavera H, Aguilar Z, Calderón D, Chlieh M, Sekiguchi T, Nakai S, and Yamazaki F (2012): Mega-Earthquakes Rupture Scenarios and Strong Motion Simulations for Lima, Peru. *The International Symposium for CISMID 25th Anniversary Technological Advances and Learned Lessons from Last Great Earthquakes and Tsunamis in the World*, Paper No. TS-6-2, Lima, Peru.

[5] CISMID (2005): Study of the Vulnerability and Seismic Risk in 42 districts of Lima and Callao. *Japan - Peru Center for Earthquake Engineering Research and Disaster Mitigation*, National University of Engineering, Lima, Peru (in Spanish).

[6] CISMID (2010): Seismic Microzonation of 6 districts in Lima. *Japan - Peru Center for Earthquake Engineering Research and Disaster Mitigation*, National University of Engineering, Lima, Peru (in Spanish).

[7] Calderon D, Sekiguchi T, Nakai S, Aguilar Z and Lazares F (2012): Study of Soil Amplification Based on Microtremor and Seismic Records in Lima Peru, *Journal of Japan Association for Earthquake Engineering*, Vol. 12, No. 2, 2012.

[8] Cabrejos J (2013): *Amplificación Sísmica en la Ciudad de Lima aplicando la técnica de Cocientes Espectrales* (Tesis de Pregrado). Universidad Nacional de Ingeniería, Lima, Perú (In Spanish).

[9] Quispe S, Yamanaka H, Aguilar Z, Lazares F, and Tavera H (2013): Preliminary Analysis for Evaluation of Local Site Effects in Lima city, Peru from Ground Motion Data by Using the Spectral Inversion Method. *Journal of Disaster Research*, Vol. 8 No. 2, pp. 243 – 251.

[10] Iwata T and Irikura K (1988): Source parameters of the 1983 Japan Sea Earthquake sequence. *J. Phys. Earth*. 36, pp. 155-184.

[11] Repetto P, Arango I, and Seed H B (1980): Influence of site characteristics on building damage during the October 3, 1974 Lima earthquake, *Report-Earthquake Engineering Research Center*, College of Engineering, University of California, Berkeley, California, NTIS, 80–41.

[12] Le Roux JP, Tavares C, and Alayza F (2000): Sedimentology of the Rímac-Chillón alluvial fan at Lima, Peru, as related to Plio-Pleistocene sea-level changes, glacial cycles and tectonics. *Journal of South American Earth Sciences*, 13, 499–510.

[13] Quispe S, Chimoto K, Yamanaka H, Tavera H, Lazares F, and Aguilar Z (2014): Estimation of S-Wave Velocity Profiles at Lima city, Peru using Microtremor Arrays. *Journal of Disaster Research*, Vol. 9 No. 6, pp. 931 – 938.

[14] Calderon D (2012): *Dynamic characteristics of the soils in Lima, Peru, by estimating shallow and deep shear-wave velocity profiles* (Doctoral thesis). Graduate School of Engineering, Chiba University, Japan.

[15] Martínez A and Porturas F (1975): Planos Geotécnicos para Lima, Perú, Análisis y Visión en Ingeniería Sísmica. *Pontificia Universidad Católica del Perú*, Lima, Perú (In Spanish).

[16] Husid L R (1969): Características de Terremotos – Análisis General. *Revista del IDIEM 8*, pp. 21 – 42, Santiago, Chile (In Spanish).

[17] McCann MWJ and Shah HC (1979): Determining strong motion duration of earthquakes. *Bulletin of Seismological Society of the America*, Vol.69, pp. 1253 – 1265.

[18] Takemura M, Ikeura T, and Sato R (1990): Scaling relations for source parameters and magnitude of Earthquake in the Izu Peninsula Region. *Tohoku Geophys. J.* (Sci. Rep. Tohoku Univ., Ser. 5), Vol.32, pp. 77 – 89.

[19] Riepl J, Bard PY, Hatzheld D, Papaionnou C, and Nechtschein S (1998): Detail evaluation of site-response estimation methods across and along the sedimentary valley of Volvi (EURO-SEISTEST). *Bulletin of the Seismological Society of America*, Vol. 88, No. 2, pp. 488–502.

[20] Lawson CL and Hanson RJ (1974): *Solving least squares problem*. New Jersey: Prentice-Hall, Inc., Englewood Cliffs, 1–337.

[21] Takemura M, Kato K, Ikeura T, and Shima E (1991): Site amplification of S-waves from strong motion records in special relation to surface geology. *Journal of Physics of the Earth*, 39, pp. 537 – 552.

[22] Yamanaka H, Nakamura A, Kurita K, and Seo K (1998): Evaluation of site effects by an inversion of S-wave spectra with a constraint condition considering effects of shallow weathered layers. *Zisin (Journal of the Seismological Society of Japan)*, Vol. 51, pp. 193 – 202 (In Japanese with English Abstract).

[23] Yamanaka H, Ohtawara K, Grutas R, Tiglao RB, Lasala M, Narag IC, and Bautista, B. C. (2011): Estimation of site amplification and S-wave velocity profiles in metropolitan Manila, the Philippines, from earthquake ground motion records. *Exploration Geophysics*, Vol. 42, pp. 69 – 79.

[24] Nakamura Y (1989): A Method for Dynamic Characteristics Estimation of Subsurface using Microtremor on the Ground Surface, *Quarterly Report of Railway Technical Research Institute (RTRI)*, Vol. 30, No.1, pp. 25 – 33.

[25] Kanamori H (1972): Mechanism of Tsunami Earthquakes. *Phys. Earth Planet*, Inter., 6, pp. 346 – 359.

[26] Brune JN (1970): Tectonic Stress and the Spectra of Seismic Shear Waves from Earthquakes. *Journal of Geophysical Research*, Vol. 75, No. 26, pp. 4997 – 5009.

[27] Sekiguchi T, Calderon D, Nakai S, Aguilar Z, and Lazares F (2013): Evaluation of Surface Soil Amplification for Wide areas in Lima, Peru. *Journal of Disaster Research*, Vol. 8, No. 2, pp. 259–265.

[28] Espinoza AF, Husid LR, Algermissen ST, and De Las Casas J (1977): The Lima earthquake of October 3, 1974: Intensity Distribution. *Bulletin of the Seismological Society of America*, Vol. 67, No. 5, pp. 1429 – 1439.